

Numerical Simulation of Blast Effects on Fibre Grout Strengthened RC Panels

Corneliu Cismaşiu^{1,a}, H. B. Rebelo^{1,2,b*}, V. J. G. Lúcio^{1,c}, M. T. M. S. Goncalves^{3,d},
G. J. Gomes^{2,e} and J. P. F. Basto^{2,f}

¹CERIS, ICIST and Departamento de Engenharia Civil, Faculdade de Ciências e Tecnologia,
Universidade NOVA de Lisboa, Portugal

² CINAMIL, Academia Militar, Lisboa, Portugal

³Departamento de Engenharia Civil, Faculdade de Ciências e Tecnologia, Universidade NOVA de
Lisboa, Portugal

^acornel@fct.unl.pt, ^bh.rebelo@campus.fct.unl.pt, ^cvjgl@fct.unl.pt, ^dmanel_goncalves@hotmail.com,
^egomes.gj@mail.exercito.pt, ^fbasto.jppof@mail.exercito.pt

Keywords: Non-linear dynamic analysis; Applied Element Method; Blast effects; Fibre reinforced grout

Abstract. The present paper aims to examine the potential of the Applied Element Method (AEM) in simulating the blast effects in RC panels. The numerical estimates are compared with the results obtained in an experimental campaign designed to investigate the effectiveness of fibre grout for strengthening full scale RC panels by comparing the effects that a similar blast load produces in a reference and the strengthened panel. First, a numerical model of the reference specimen was created in the software *Extreme Loading for Structures* and calibrated to match the experimental results. With no further calibration, the fibre reinforced grout strengthening was added and the resulting numerical model subjected to the same blast load. The experimental blast effects on both reference and strengthened panels, despite the lack of high speed measurement equipment (pressure, strains and displacements sensors), compare well with the numerical estimates in terms of residual and maximum displacements, showing that, once calibrated, the AEM numerical models can be successfully used to simulate blast effects in RC panels.

Introduction

Ever since Humankind began to build structures, they were always designed to withstand a broad set of loads, e.g. gravity, wind, temperature changes and earthquakes. However, over the last few decades, wars, terrorist attacks and accidental explosions, established the need to consider blast loads in the design of important structures [1]. Research on the effects of blast loads is essential for the successful design of blast resistant structures. Nevertheless, experimental testing is expensive, as can only be conducted in a highly controlled and safe environment. Alternatively, one might resort to computational models based on simplified or complex numerical formulations, able to simulate the highly non-linear dynamic response, typical to blast scenarios. To be reliable, these numerical simulations must be validated through experimental field tests, as illustrated in recent publications, e.g. [2–5]. Results from field blast tests are used in the present paper to inquire the potential of a numerical model based on the AEM to simulate the dynamic non-linear response of RC panels to overpressures produced by unconfined free-air explosions.

Full scale experimental blast tests

A full scale experimental campaign, part of the “*Strategic building structural security and integrity, against accidental or deliberate explosions*” (SI4E) research project [6], designed to analyse the effectiveness of fibre reinforced grout strengthening in RC panels, was conducted in Santa Margarida military camp according to the rules and safety procedures approved by the Portuguese Army.

RC panels. Blast tests were performed on two RC panels, having the same dimensions of $2.60 \times 2.17 \times 0.12$ m. The panels were obtained from a unique, larger, façade element and therefore were characterized by the same reinforcement detailing, which consists on one NC50 steel mesh in each face ($\phi 5@100$ mm in the longitudinal direction and $\phi 5@150$ mm in the transversal direction) and $2\phi 12$ rebars on three of the edges. While one of the panels was kept as reference, the other one was strengthened using a layer of 20 mm thick unidirectional fibre reinforced grout (UFRG), having a content of 1% longitudinal continuous steel fibres. Both the reference and the strengthened panels are illustrated in Figure 1.

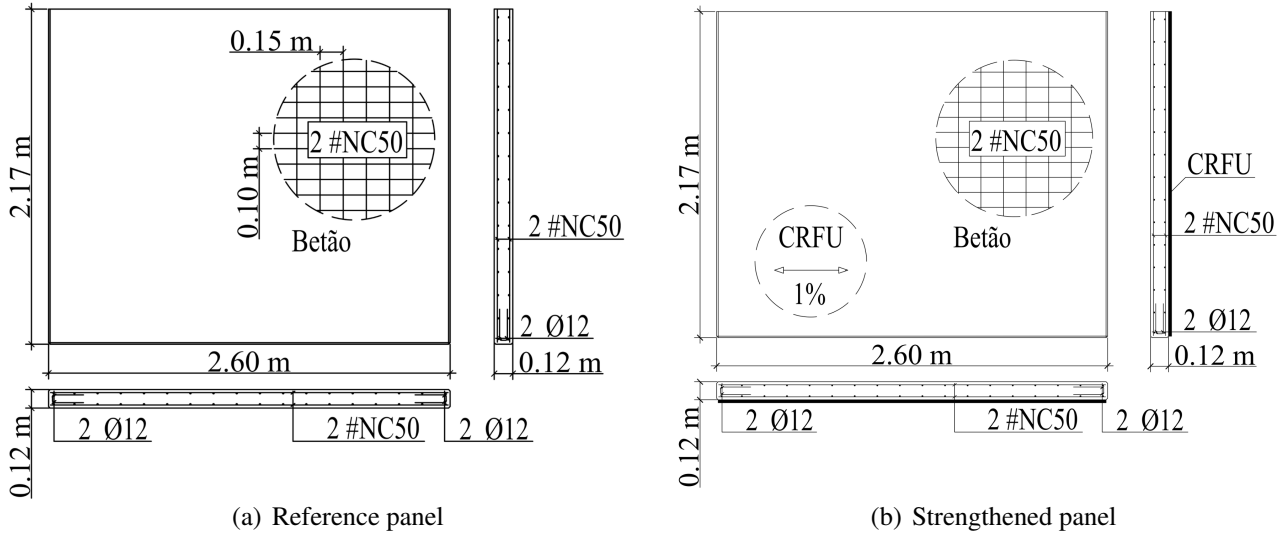


Fig. 1: Detailing of the experimental panels

As collected in Table 1, concrete with an average compression strength at 28 days of 46 MPa in 150 mm cube specimens was used for the two panels. A $f_{yk} = 500$ MPa steel was used for the rebars and the reinforced meshes. According to [7], the matrix composition of the UFRG used in the strengthened panel (75% Portland cement type I class 42.5R, 2% Silica fume, 0.5% Sika ViscoCrete 3005, 22.5% water), presents a high mechanical resistance and controlled shrinkage. Its failure stresses in tension and compression were identified to 5.8 and 78.8 MPa, respectively.

Table 1: Experimental model material properties

Material	Properties	
Concrete	$f_{cm} = 46.0$ MPa	n/a
Steel	n/a	$f_{yk} = 500.0$ MPa
UFRG	$f_{cm} = 78.8$ MPa	$f_{ctm} = 5.8$ MPa

During the blast tests, the RC panels were supported on concrete beams with 0.3 m width, resulting in simply supported slab configurations with a theoretical span of 2.45 m. The strengthened model was positioned with the UFRG layer on the opposite side with respect to the blast load, in order to improve the model resistant and ductility due to the presence of fibres on the UFRG. The explosive charge, 8 kg of TNT, was suspended 3 m above the model, aligned with its centre, as illustrated in Figures 2(a) and 2(b).

Preliminary estimation of the mid-span maximum deflection. A preliminary prediction of the maximum displacements at mid-span is essential in the planning phase of the experimental tests, as it allows to choose an explosive charge sufficiently high to generate visible damage in the panels but, at the same time, small enough to avoid their total collapse.

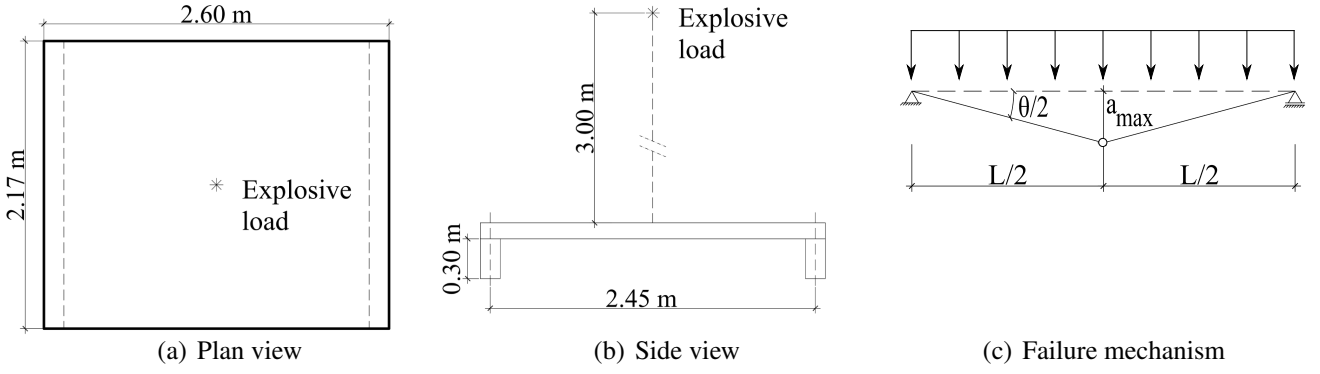


Fig. 2: Blast test setup and simplified failure mechanism

The shock wave resulting from the free-air burst of the considered explosive charge, yields a scaled distance ($z = R/W_{TNT}^{1/3}$) at the mid-span of the panel of $1.5 \text{ m/kg}^{1/3}$. The corresponding reflected specific impulse (i_r), needed in the computation of the total impulsive load on the panel, can be estimated [8] as a function of the specific impulse (i_s) and the peak of the incident and reflected overpressures (P_{so} and P_r),

$$i_r \simeq i_s \frac{P_r}{P_{so}}. \quad (1)$$

The necessarily free-field parameters can be readily obtained using the empirical formulation presented by Kinney and Graham. According to [9], the specific impulse can be estimated as a function of the scaled distance as,

$$i_s = \frac{0.0067 \sqrt{1 + (z/0.23)^4}}{z^2 \sqrt[3]{1 + (z/1.55)^3}} = 0.102 \text{ MPa}\cdot\text{ms}. \quad (2)$$

and the peak incident overpressure is defined as a function of the atmospheric pressure (P_a) and the scaled distance,

$$P_{so} = \frac{808 [1 + (z/4.5)^2] P_a}{\sqrt{1 + (z/0.048)^2} \sqrt{1 + (z/0.32)^2} \sqrt{1 + (z/1.35)^2}} = 0.406 \text{ MPa}. \quad (3)$$

The peak reflected overpressure can be computed as a function of the peak of the incident overpressure and the atmospheric pressures using the Rankine-Hugoniot relation given in [10],

$$P_r = 2P_{so} \left(\frac{7P_a + 4P_{so}}{7P_a + P_{so}} \right) = 1.699 \text{ MPa}. \quad (4)$$

Introducing the numerical values computed in Eqs. (2) to (4) in definition (1), the reflected specific impulse can readily be obtained as $0.428 \text{ MPa}\cdot\text{ms}$.

Next, the load on the exposed surface of the reference panel (I_r) can be estimated considering the blast load at the mid-span of the panel as an equivalent uniform load over the whole panel [11],

$$I_r = i_r \times \text{panel surface} = 0.428 \times 2.45 \times 2.17 = 2.275 \text{ kNs}. \quad (5)$$

Considering a failure mechanism with a plastic hinge at mid-span, see Figure 2(c), and assuming an equivalent SDOF dynamic system to represent the response of the blast-loaded panel, its equivalent mass ($M_{eq} = K_{LM} M_{panel}$) can be estimated using the load-mass factor ($K_{LM} = 0.66$) defined in [11]

and the mass of the blast-loaded panel ($M_{panel} = 1.595$ ton). The resulting kinetic energy induced by the blast can be estimated as,

$$T = I_r^2 / (2M_{eq}) = 2.460 \text{ kJ.} \quad (6)$$

Assuming a perfectly plastic behavior of the panel under blast loading (yield displacement at mid-span considered to be small when compared to its maximum value), the energy dissipated by the plastic deformation of the panel can be computed as,

$$W = M_r \theta_{max} = 4 M_r a_{max} / L. \quad (7)$$

where M_r , θ_{max} , a_{max} and L represent the bending moment capacity of the section, mid-span rotation discontinuity, mid-span displacement and panel span, respectively, as illustrated in Figure 2(c). Assuming a plastic behavior of the reinforcement after yielding, a rectangular stress distribution for concrete in the compression zone and neglecting the compression in the rebars, the moment capacity of the section can be computed as,

$$M_r = \rho f_y d^2 \left(1 - \frac{\rho f_y}{2 f_c} \right). \quad (8)$$

For the reference panel, based on the material properties and the reinforcement detailing, the following numerical values were considered: 0.0022 for the reinforcement ratio (ρ), 500 MPa (characteristic value for the steel resistance class) for yield strength of reinforcement (f_y), 0.0875 m for the effective depth (d) and 36.8 MPa for the mean compressive strength of concrete in cylinder specimens, yielding a moment capacity of 18.3 kNm. One mention that the strain rate effects were not considered on this preliminary estimation in order to keep these computations as simple and straightforward as possible.

Considering that the kinetic energy induced by the blast load (6) is dissipated by the plastic deformation of the panel (7), one can readily compute the maximum mid-span displacement, $a_{max} = 82$ mm. Note that, due to energy dissipation in the supports, related to the damping capacity of the soil, a slightly smaller value is expected in the experimental blast test.

Maximum and residual mid-span displacements. The maximum and the relative residual displacements in the mid-span of the RC panels are used as a measure of the blast effects. While the relative residual displacements can be readily obtained using a 2 m ruler and a tape measurer, see Figure 3(a), recording of the absolute maximum displacements is much more challenging.

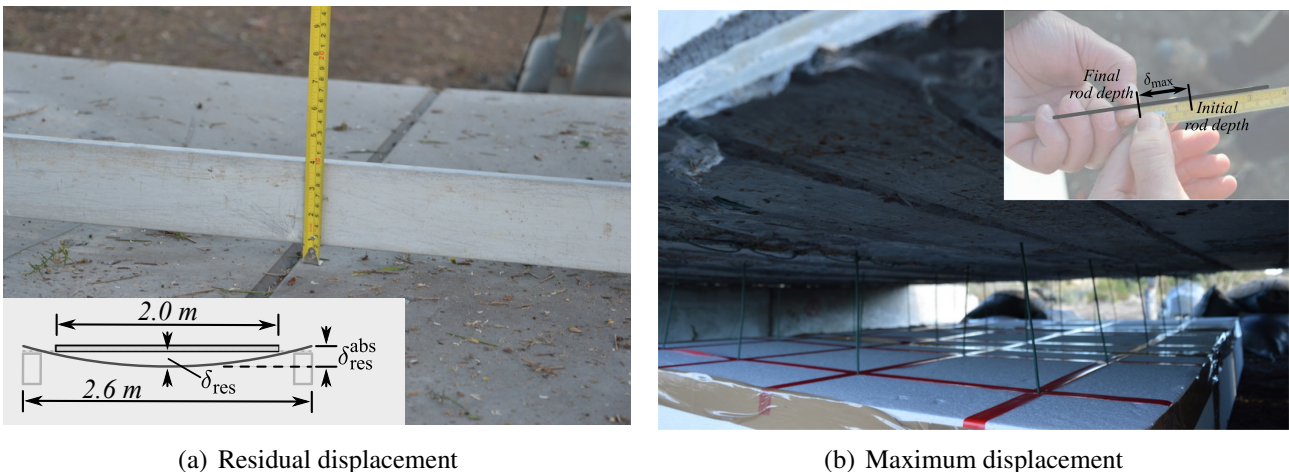


Fig. 3: Recording of the mid-span displacements of the RC panel

A polystyrene plate was fixed under the RC panel and several metallic rods, 200 mm long, were pinned into it, in close contact with the panel, see Figure 3(b). During the blast, the maximum deflection of the panel drove the rods deeper into the polystyrene. The difference between the initial and final rod depth, see top right image in Figure 3(b), is directly associated to the maximum deflection of the panel.

Experimental results. The effects of the blast detonation in the RC panels were analyzed in terms of residual and maximum mid-span displacements. As expected, both the maximum 65 mm and residual 20 mm mid-span displacements for the reference panel were larger than their counterparts measured for the strengthened panel, measuring 33.5 and 10 mm, respectively. Note that, as expected, the initial estimate for the maximum mid-span displacement of the reference panel previously computed overestimates the experimental value. The 26% difference is considered acceptable, taking into account the simplicity of the analytical model.

Numerical simulation of the blast effects

To examine the potential of the AEM in simulating the blast effects in RC panels, the experimental tests are simulated numerically in the software *Extreme Loading for Structures* (ELS) [12]. The program, providing a full non-linear dynamic analysis based on the AEM [13–16], have been already used successfully to simulate the response of structures subjected to severe loading related to earthquakes, progressive collapse or blast [17–21], among others.

Introduction to the AEM. In the AEM [13, 14] the structural elements are virtually divided into an assembly of small rigid elements, connected to each other by pairs of normal and shear springs distributed along the common interface. Considering the applied loading, the stresses and the corresponding strains can be readily computed in all springs. Adopting fully non-linear constitutive models to simulate the behavior of the structural materials, the maximum forces that the springs can resist can be determined. Once these force levels are reached, anywhere within the model, the corresponding springs are cut, simulating a crack initiation or propagation, with no need of an *a priori* knowledge of the crack location. If all springs connecting an element are cut, separation occurs and eventual sub-sequential collisions, contact and re-contact between elements are automatically considered.

Numerical models. Numerical models for both the reference and the UFRG strengthened RC panel were developed in ELS. First, the non-linear constitutive models must be calibrated to match the properties of the materials used in the experimental tests. Next, the geometry of the panels must be accurately modelled, with special care to reinforcement detailing, mesh sensitivity and boundary conditions.

Material calibration. The constitutive model implemented in ELS to simulate concrete under compression stresses is the Maekawa's elasto-plastic and fracture model [22], characterized by the initial Young's modulus, the fracture parameter and the compressive plastic strain. Additionally, in order to consider the confinement effects in compression zones, Kupfer's [23] biaxial failure function is considered. Alternatively, linear stress-strain relations are adopted for concrete subjected to tension and shear stresses, until the ultimate tension is reached. To calibrate relevant parameters for the concrete, compression tests conducted on 150 mm size cubes samples, were numerically simulated and the resulting compressive strength was compared with the 46 MPa experimental mean compressive strength ($f_{cm,cube}$). Additional parameters used in the constitutive model, were a Poisson's ratio of 0.2 and values given in the EC2 [24] for the mean secant modulus of elasticity (E_{cm}) 33 GPa, the mean tensile strength (f_{ctm}) 2.90 MPa, the strain at maximum compression stress (ε_{c1}) and the ultimate compression strain (ε_{cu1}), 2.2 and 3.5‰, respectively. The plot presented in Figure 4(a) represents the numerical simulation of the compression tests in the cubic samples using the calibrated constitutive model for concrete.

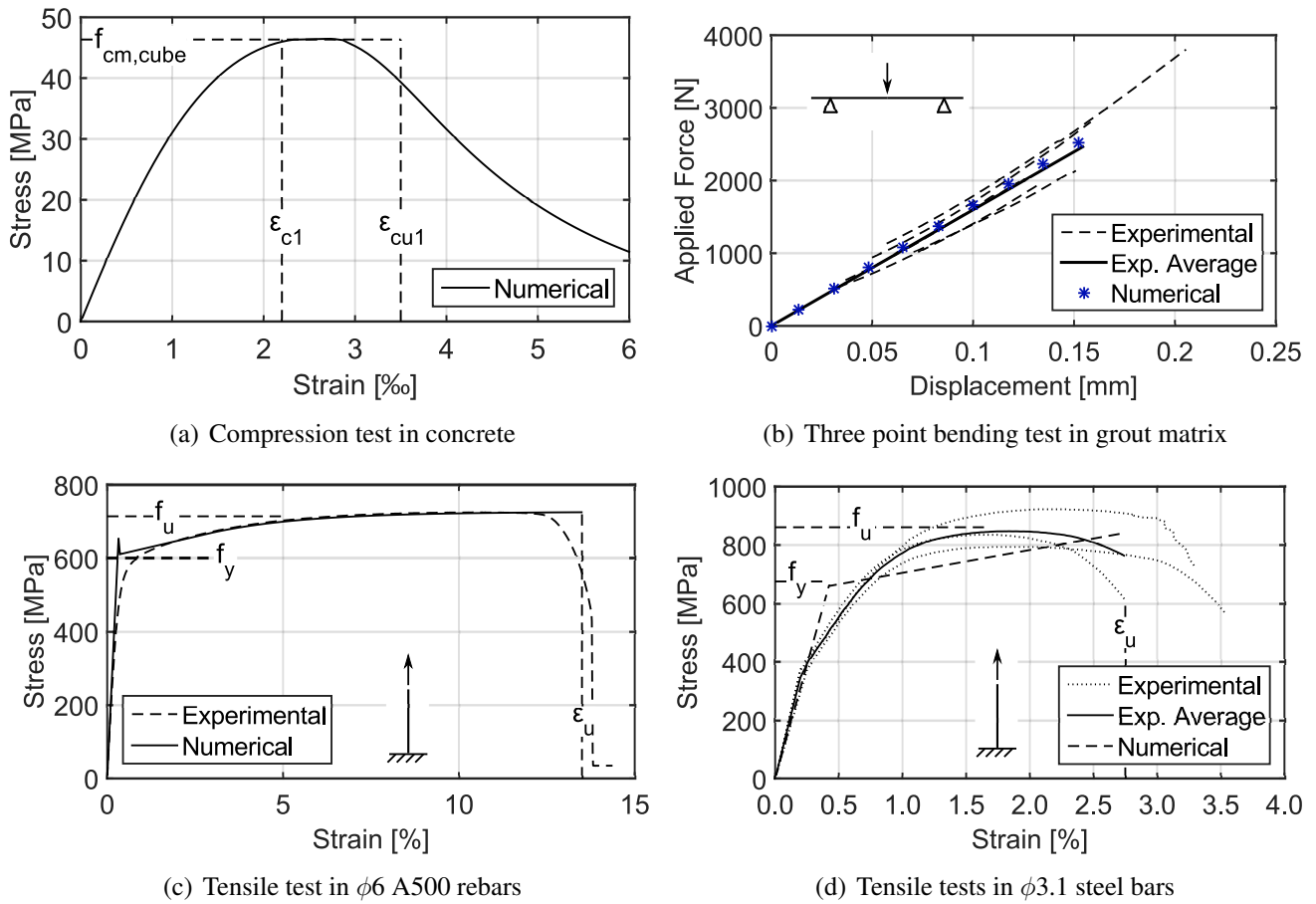


Fig. 4: Calibration of the material constitutive models

The same constitutive model was used to simulate the structural behaviour of the grout matrix used in the UFRG. Results of experimental compression and three point flexural tests were used to identify the relevant parameters, namely the mean secant modulus of elasticity (E_{cm}) 2279 MPa, the mean compressive strength (f_{cm}) 78.8 MPa and the mean tensile strength (f_{ctm}) 5.8 MPa. The force-displacement diagram, obtained in a numerical simulation of three point bending tests using the calibrated constitutive model for the grout matrix, is plotted in Figure 4(b) against the experimental values.

The Ristic constitutive model [25] is implemented in ELS in order to characterize the behavior of the reinforcement bars. Using this model, the tangent stiffness in a rebar spring depends on the current strain, the loading status (loading or unloading) and the previous loading history which controls the Bauschinger's effect. One must note however, that the ELS does not consider the buckling of the reinforcement bars [15]. The results of tensile tests performed experimentally on $\phi 6$ A500ER reinforcement bars, were used to calibrate the model parameters. A sensitivity analysis yield values of 200 and 76.9 GPa for the elastic (E_a) and shear (G_a) modulus, 600 MPa for the tensile yield stress (f_y), 1.19 for the ratio between the ultimate strength and the tensile yield stress (f_u/f_y), 13.5% for the ultimate strain (ϵ_u) and 0.011 for the post yield stiffness ratio (E_y/E_a). The corresponding numerical and experimental stress-strain curves are plotted in Figure 4(c).

The structural behaviour of the $\phi 3.1$ mm steel wires, from which the steel fibremat used in the UFRG was produced, is simulated using the same Ristic constitutive model. Tensile experimental tests reported in [7] are used to calibrate its relevant parameters, yielding values of 160 and 61.5 GPa for the elastic (E_a) and shear (G_a) modulus, 675 MPa for the tensile yield stress (f_y), 1.275 for the ratio between the ultimate strength and the tensile yields stress (f_u/f_y), 2.75% for the ultimate strain (ϵ_u) and 0.05 for the post yield stiffness ratio (E_y/E_a). The corresponding numerical and experimental stress-strain curves are plotted in Figure 4(d).

Geometry and element mesh. The reference panel used in the experimental blast tests was a $2.60 \times 2.17 \times 0.12$ m rectangular element. As illustrated in Figure 5(a), the panel was modelled using a regular mesh consisting of 15480 ($86 \times 45 \times 4$) 8 nodes elements, connected to each other by 5×5 pairs of normal and shear springs distributed along each common interface. The reinforcement bars were defined according to the panels' detailing, see Figure 5(b). A mesh sensitivity analysis was performed in order to guarantee the convergence of the numerical solution for the adopted mesh.

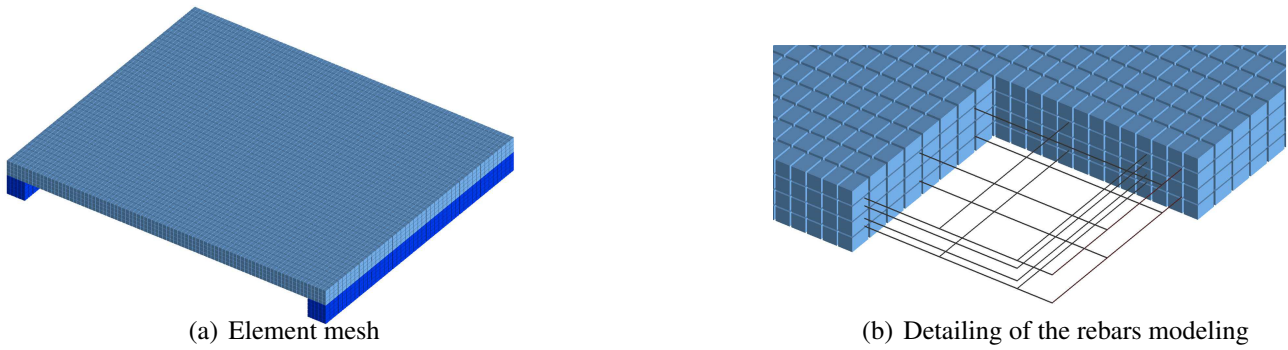


Fig. 5: Numerical model of the RC reference panel

The reinforced panel had an identical geometry as the reference one, except for the 20 mm thick layer of UFRG. This layer was modeled using 3870 ($86 \times 45 \times 1$) additional 8 node elements. The steel fibres embedded into the cement-based grout were simulated using uniformly distributed (5×5) $\phi 0.7$ mm reinforcement bars oriented along the fibres direction, see Figure 6, ensuring the 1% content of longitudinal steel fibres [7].

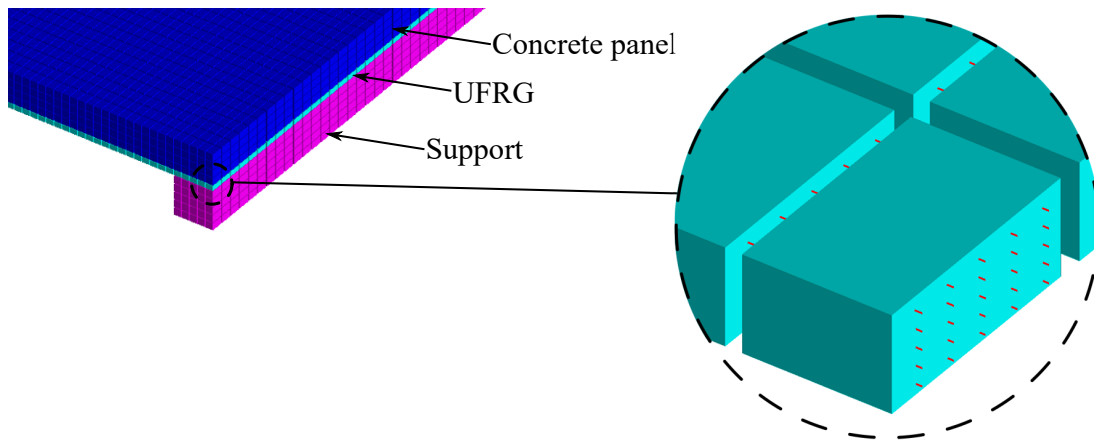


Fig. 6: Steel fibres in the UFRG reinforcement layer

Preliminary boundary conditions. It is well known that enforcing the correct boundary conditions is extremely important in order to get accurate solutions in dynamic analysis. In the experimental blast tests, the panels were simply supported on concrete beams, firmly seated on the soil surface. While simply supported conditions between the panels and the beams can readily be ensured, the boundary conditions to be enforced at the base of the beams are not evident, due to uncertainties regarding the soil properties. Therefore, a preliminary analysis was performed assuming clamped conditions between at the base of the beams.

Selected time step. Due to the almost instantaneous rise of pressures as a result of the detonation, the numerical simulation of the blast tests requires very small time steps to ensure an accurate representation of the loading pressure and a stable numerical integration. After a sensitivity analysis,

the first 0.05 s of the analysis, roughly the duration of the positive phase of the blast wave, was computed using a time step of 10^{-4} s. To reduce to total time required by a 2 s analysis of the structural response of the panels, the next 1.95 s were computed using a time step of 10^{-3} s. On an Intel Xeon CPU 5670 at 2.93 GHz with 16 GB of RAM, the 2450 time steps corresponding to a 2 s time history of the structural response, required between 8 to 10 hours to complete.

Simulation of the blast effects on the reference panel

In order to compare the numerical estimates with the experimental results, the numerical model of the reference panel was subjected to a 8 kg TNT explosive charge at 3 m of distance. The pressure time history, applied to the elements facing the explosive charge, is determined through empirical correlations based on CONWEP, as presented in [12]. The resulting mid-span relative displacement (measured as illustrated in Figure 3(a)) time history, is illustrated as curve (i) in Figure 7, together with the value of the residual displacement (δ_{res}) measured experimentally in the field test. This plot indicates that the numerical mid-span residual displacement is still far from the experimental value. To improve the simulation, three important aspects must be included in the numerical model. They are related to (a) size of the contact surface between the panel and concrete beams, (b) elasticity and damping of the boundary conditions due to the presence of the soil and (c) strain rate effects affecting the material properties for dynamic loading.

Size of the contact surface. To control the contact area during collisions, a so called normal contact stiffness factor (N_F) is defined in ELS. According to the ELS manual [12], its value is directly proportional with the average contact area between the elements. A relatively small value is recommended for stiff materials such as concrete, leading to relatively small contact areas and therefore, high associated stresses. However, in the performed blast simulation, the high stresses associated to the default value suggested for concrete elements, $N_F = 0.01$, led to failure of the panels near to supports, phenomenon that was not observed during the experimental tests. To improve the results, a unitary normal contact stiffness factor was assumed.

Elasticity and damping of the boundary conditions. One recall that in this preliminary numerical simulation, clamped conditions were assumed to the base of the concrete beams. However, the curve (i) in Figure 7 suggest that, part of the blast energy was dissipated by the damping properties of the soil. Therefore, to improve the numerical estimates, the boundary conditions must include the soil effects. As an explicit modelling of the soil would considerably increase the computational effort, its influence was incorporated in the numerical model using a virtual equivalent material for the clamped supporting beams, calibrated to incorporate the elasticity of the soil and its damping properties.

To find the elastic modulus of this equivalent material, the response of the supports to vertical loads was assumed to be identical to the one simulated in a numerical model that includes the concrete beams and the surrounding soil. Considering a type D soft-to-firm cohesive soil [26], with an elastic modulus estimated based on the results of a standard penetration test ($N_{SPT} = 15$) [27],

$$E_{soil} = N_{SPT} (0.84 + 0.036 N_{SPT}) = 20.7 \text{ MPa.} \quad (9)$$

the elastic modulus of the equivalent material to be used in the supports yields 9 MPa.

In ELS, the capacity of the elastic supports to dissipate energy is defined through a so called damping factor (r), which can be computed as a function of the natural frequency of the supports (ω) and the desired damping ratio (ζ),

$$r = 2 \omega \zeta. \quad (10)$$

Assuming, for the support beams, an elastic material having the equivalent elastic modulus and a critical damping, the corresponding damping factor yields $r = 9071 \text{ s}^{-1}$.

The improvements in the numerical estimates for the time-history of the mid-span displacements are clearly illustrated in Figure 7 where, besides the original numerical estimates obtained using clamped concrete beam supports, curve (i), one can observe the influence of taking into account the size of the contact surface and the equivalent elastic material to include soil elasticity, curve (ii) and, finally, damping effects, curve (iii). Recall that δ_{res} in Figure 7 represents the value of the mid-span residual displacement measured experimentally in the field test.

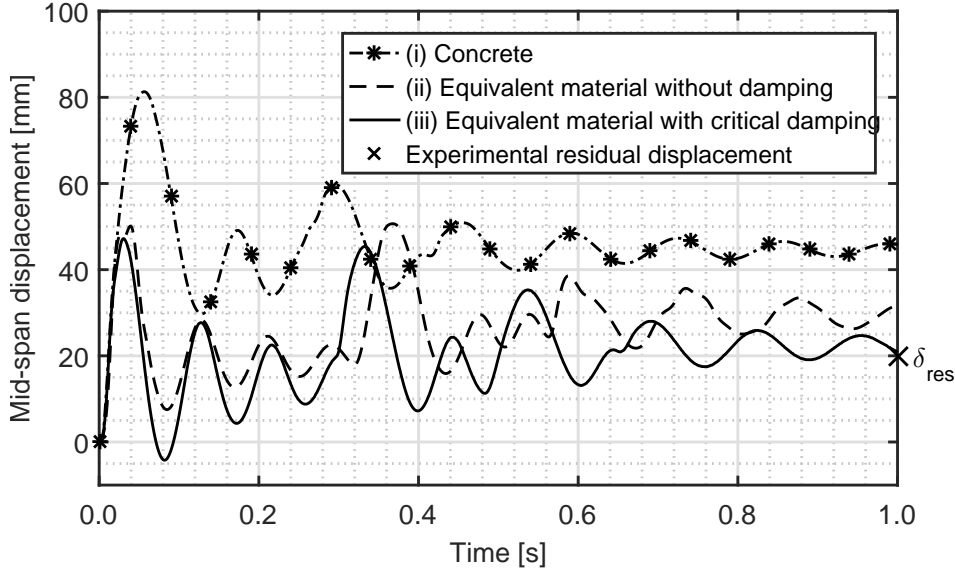


Fig. 7: Relative mid-span displacement time history

Strain rate effects. When subjected to high speed dynamic loads, the apparent strength of materials can increase significantly. The dynamic increase factor (DIF), i.e. the ratio of the dynamic to static strength, is normally given as function of strain rate [28–30]. To incorporate the strain rate effects in the analysis, the DIFs are estimated iteratively: first, assuming unitary DIFs, the dynamic analysis is performed in order to obtain an estimate for the strain rates and the DIFs are updated accordingly; with the updated DIFs, the analysis is performed again, yielding new strain rates and, consequently, new DIFs. This procedure is repeated until no significant changes are recorded between two analyses.

The expressions given in [30] and [29] were used in the present paper to express the strain rate dependency of the relevant material parameters for concrete, Figure 8(a), 8(b) and 8(c) and steel, Figure 8(d), respectively. Note that, according to Malvar and Crawford [29], the elastic modulus of steel remains constant regardless of the strain rate.

The resulting DIFs used in the numerical simulations to take into account the strain rate effects are given in Table 2 for the reference and strengthened panels.

Table 2: Computed DIFs

Material	Property	Reference panel	Strengthened panel
Concrete	f_{cm}	1.40	1.35
	f_{ctm}	1.59	1.53
	E_{cm}	1.35	1.32
Steel	f_y	1.32	1.31
	f_u	1.09	1.09

Final estimates for the mid-span maximum and residual displacements. The resulting estimates for the absolute and relative residual mid-span displacements time history are plotted in Fig-

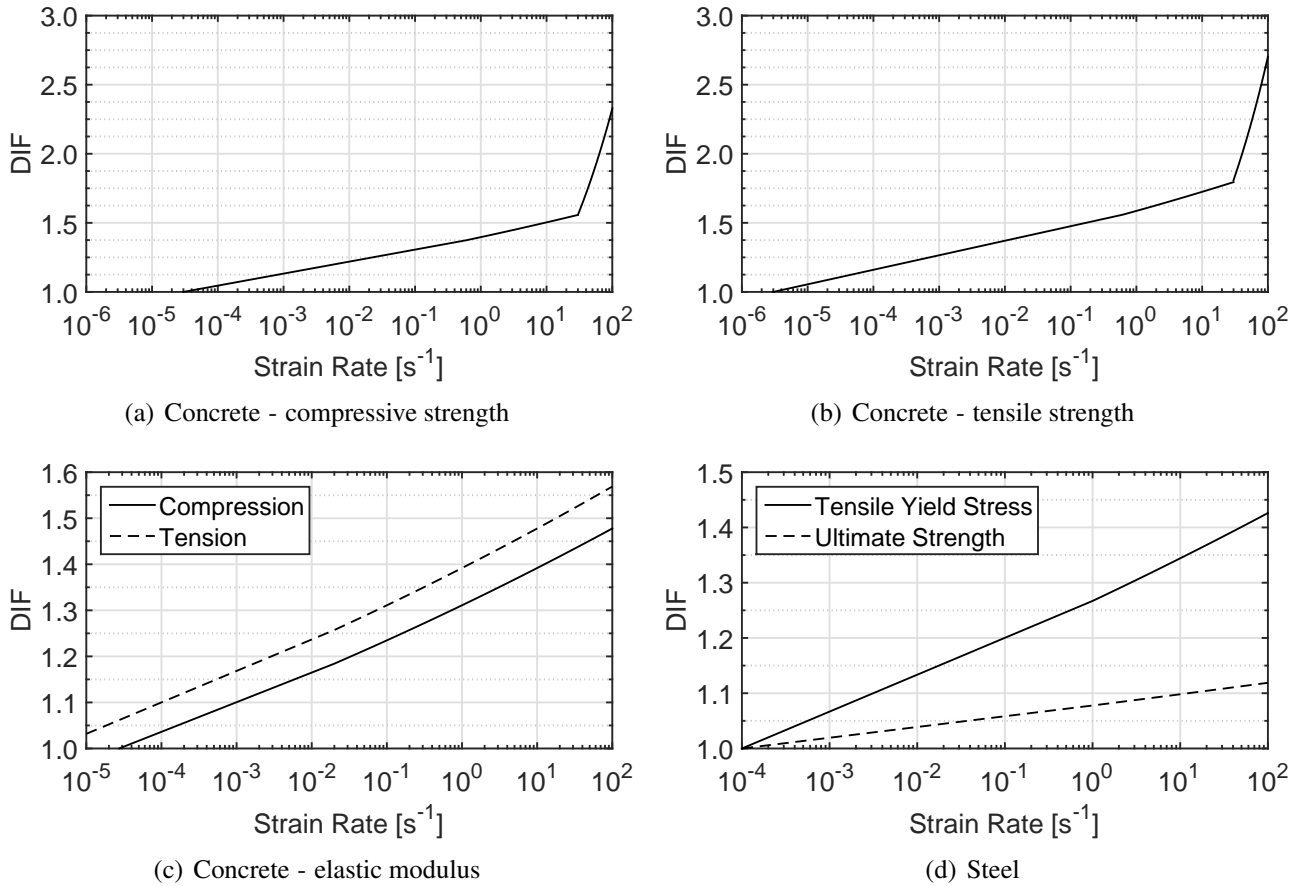


Fig. 8: Dynamic Increase Factor as a function of the strain rate

ure 9(a) and 9(b), together with the values measured experimentally in the field tests for the maximum (δ_{max}) and residual (δ_{res}) mid-span displacements.

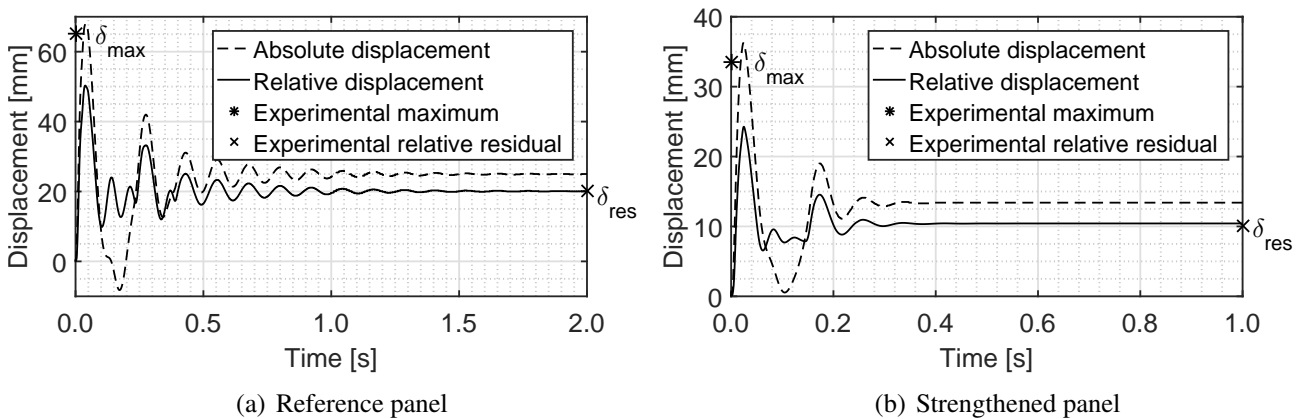


Fig. 9: Numerical and experimental mid-span absolute and relative displacements

Analysing the plots in Figure 9 one can conclude that the numerical estimates for both the reference and the strengthened panel produce accurate results. The mid-span displacement time history for the reference panel given in Figure 9(a) exhibits a relative error of 4% for the maximum value, while the residual displacement is recover exactly. One note that, as the numerical model was calibrated using the experimental value of the residual displacement of the reference panel, this result was expected. However, one must note also that the numerical model is able to recover the value of the mid-span absolute maximum displacement as well, although the corresponding experimental value was not used during the calibration of the numerical model. Moreover, the reliability of the numerical

model is confirmed when analysing the estimates for the strengthened panel, Figure 9(b). Note that, to model the strengthened panel, the UFRG layer was simply added to the reference model and the DIFs actualized to match the corresponding strain rates. In this case, the relative error is 10% in the maximum displacements and 4% in the residual mid-span displacements. These slightly larger errors in the numerical estimates were expected, and may be a consequence of (i) inaccurate modelling of the fibremat inside the grout (considered as regular rebars with perfect adherence) and (ii) uncertainties related to the blast waves (no experimental measurements available) and soil conditions between the two blast events (first blast might have mildly change the soil conditions).

Conclusions

The objective of the present paper was to examine the reliability of numerical models based on the AEM, when used to simulate the structural response of RC panels subjected to the blast effects of unconfined detonations. The simulations, once the corresponding numerical models calibrated, yield accurate solutions when compared with the results of full scale experimental tests.

Based on the results reported in this paper, one can conclude that, in order to obtain trustworthy numerical models for blast simulations, it is extremely important to perform experimental measurements that can be used to define reliable boundary conditions, both in what respect their elasticity and damping properties. Moreover, the lack of high speed measurement equipment (pressure, strains and displacements sensors) might hinder the comparison between experimental and simulated estimates.

Despite the mentioned limitations, one can conclude that numerical models based on the AEM can accurately predict and simulate the structural response of fibre reinforced grout strengthened RC panels when subjected to blast effects.

Acknowledgements

This work is part of the research developed in the Department of Civil Engineering of the Faculty of Science and Technology of NOVA University of Lisbon in cooperation with the Portuguese Military Academy within the SI4E research project. Cooperation with our colleagues from Regimento de Engenharia No.1 CEng/BrigMec is gratefully acknowledged, as well as the courtesy of the precast company Concremat - Prefabricação e Obras Gerais S.A. in supplying the RC panels.

References

- [1] A. Coffield and H. Adeli. An investigation of the effectiveness of the framing systems in steel structures subjected to blast loading. *Journal of Civil Engineering and Management*, 20(6):767–777, 2014.
- [2] B.D. Ellis, B.P. DiPaolo, D.L. McDowell, and M. Zhou. Experimental investigation and multi-scale modeling of ultra-high-performance concrete panels subject to blast loading. *International Journal of Impact Engineering*, 69:95–103, 2014.
- [3] H. Aoude, F.P. Dagenais, R.P. Burrell, and M. Saatcioglu. Behavior of ultra-high performance fiber reinforced concrete columns under blast loading. *International Journal of Impact Engineering*, 80:185–202, 2015.
- [4] R. Castedo, P. Segarra, A. Alañon, L.M. Lopez, A.P. Santos, and J.A. Sanchidrian. Air blast resistance of full-scale slabs with different compositions: Numerical modeling and field validation. *International Journal of Impact Engineering*, 86:145–156, 2015.

- [5] Y. Shi and M.G. Stewart. Damage and risk assessment for reinforced concrete wall panels subjected to explosive blast loading. *International Journal of Impact Engineering*, 85:5–19, 2015.
- [6] CINAMIL. <http://academiamilitar.pt/investigacao-e-inovacao/projetos.html>. Accessed: 2017-03-31.
- [7] R. Gião, V. Lúcio, C. Chastre, and A. Bras. UFRG – unidirectional fibre reinforced grout as strengthening material for reinforced concrete structures. In J. Barros, editor, *BEFIB2012 – Fibre reinforced concrete*, pages 1–12, Guimarães, 2012. University of Minho.
- [8] W.E. Baker, P.A. Cox, J.J. Kulesz, R.A. Strehlow, and P.S. Westine. *Explosion Hazards and Evaluation*. Number 5 in Fundamental Studies in Engineering. Elsevier Science, 1983.
- [9] G. F. Kinney and K. J. Graham. *Explosive Shocks in Air*. Springer Berlin Heidelberg, 2nd edition, 1985.
- [10] C.E. Needham. *Blast Waves. Shock Wave and High Pressure Phenomena*. Springer Berlin Heidelberg, 2010.
- [11] U.S. Army Corps of Engineers. *Methodology Manual for the Single-Degree-of-Freedom Blast effects Design Spreadsheets*, pdc tr-06-01 edition, September 2008.
- [12] Applied Science International, Durham, NC. *Extreme Loading for Structures V3.1. Theoretical Manual*, 2013.
- [13] H. Tagel-Din and K. Meguro. Applied element simulation for collapse analysis of structures. *Bull. of Earthquake Resistant Struct. Res. Ctr*, pages 113–123, 1999.
- [14] K. Meguro and H. Tagel-Din. Applied element method for structural analysis: Theory and application for linear materials. *Structural Engineering Earthquake Engineering*, 17(1):21–35, 2000.
- [15] K. Meguro and H. Tagel-Din. Applied element simulation of RC structures under cyclic loading. *Journal of Structural Engineering*, 127(11):1295–1305, 2001.
- [16] K. Meguro and H. Tagel-Din. Applied element method used for large displacement structural analysis. *Journal of Natural Disaster Science*, 24(1):25–34, 2002.
- [17] H. Tagel-Din and K. Meguro. Analysis of a small scale RC building subjected to shaking table tests using applied element method. *12th World Conference on Earthquake Engineering. New Zealand:[sn]*, pages 1–8, 2000.
- [18] H. Tagel-Din and K. Meguro. Applied element method for dynamic large deformation analysis of structures. *Structural Engineering Earthquake Engineering*, 17(2):215–224, 2000.
- [19] H. Tagel-Din and K. Meguro. Nonlinear simulation of RC structures using applied element method. *Structural Engineering Earthquake Engineering*, 17(2):137–147, 2000.
- [20] D. Asprone, A. Nanni, H. Salem, and H. Tagel-Din. Applied element method analysis of porous GFRP barrier subjected to blast. *Advances in Structural Engineering*, 13(1):153–170, 2010.
- [21] H. Helmy, H. Hadhoud, and S. Mourad. Infilled masonry walls contribution in mitigating progressive collapse of multistory reinforced concrete structures according to UFC guidelines. *International Journal for Advanced Structural Engineering*, 7(3):233–247, 2015.

- [22] H. Okamura and K. Maekawa. *Nonlinear analysis and constitutive models of reinforced concrete*. Gihodo Co. Ltd., Tokyo, 1991.
- [23] H. Kupfer, H. K. Hilsdorf, and H. Rusch. Behavior of concrete under biaxial stresses. *ACI Journal proceedings*, 66(8):656–666, 1969.
- [24] European Committee for Standardization (CEN). *EN1992-1-1: Eurocode 2: Design of concrete structures - Part 1-1: General rules and rules for buildings*, 2004.
- [25] D. Ristic, Y. Yamada, and H. Iemura. Stress-strain based modeling of hysteretic structures under earthquake induced bending and varying axial loads. *Research Rep. No. 86-ST*, 1, 1986.
- [26] European Committee for Standardization (CEN). *EN1998-1: Eurocode 8: Design of structures for earthquake resistance - Part 1: General rules, seismic actions and rules for buildings*, 2004.
- [27] M.A. Stroud. The standard penetration test: its application and interpretation. In *Proc. of the Conference on Penetration Testing in the UK, Birmingham*. Thomas Telford, London, 1989.
- [28] L.J. Malvar and J.E. Crawford. Dynamic increase factors for concrete. Technical report, DTIC Document, 1998.
- [29] L.J. Malvar and J.E. Crawford. Dynamic increase factors for steel reinforcing bars. In *Proceedings of the Twenty-Eighth DoD Explosives Safety Seminar*, 1998.
- [30] CEB-FIP. Design of concrete structures. CEB-FIP Model Code 1990, 1993.